SERS IMAGING OF NASOPHARYNGEAL CARCINOMA MARKERS USING AN ANTIBODY-CONJUGATED GOLD NANOPARTICLES PROBE

J.-H. Li [1*], Y. Du [2*], G.-K. Feng [2], Y.-B. Du [1], Y.-Q. Zhou [1], M.-S. Zeng [2*]

[1] School of Mechanical and Electrical Engineering, Shenzhen Institute of Information Technology, Shenzhen, 518172, China; e-mail: lijianghua25@163.com
[2] State Key Laboratory of Oncology in South China, Collaborative Innovation Center for Cancer Medicine, Department of Experimental Research, Sun Yat-sen University Cancer Center, Guangzhou, 510060, China; e-mail: zengmsh@mail.sysu.edu.cn

Surface-enhanced Raman scattering (SERS) nanotags as an ultrasensitive nanoprobe is becoming popular for the detection of biomarkers. Herein, antibody-conjugated gold nanoparticles (AuNPs) were used to target LMP2A in an LMP2A-infected CNE2 cell line. SERS maps showed that the LMP2A was distributed around the cell, which was consistent with the results of immunofluorescence staining in the previous report. This location could be due to the specific binding of the bioconjugated nanotags to the receptors on the cell surface. However, the CNE2 cell line without LMP2A-infected showed no detectable signal at 1044 cm^{-1}. The results demonstrated the potential feasibility of AuNPs nanotags as highly sensitive probes conjugated at the subcellular level for detection and localization of cancer markers in nasopharyngeal carcinoma (NPC).

Keywords: *nasopharyngeal carcinoma, LMP2A, marker probe, gold nanoparticles, CNE2.*

ПОЛУЧЕНИЕ МЕТОДОМ ПОВЕРХНОСТНО-УСИЛЕННОГО КОМБИНАЦИОННОГО РАССЕЯНИЯ СВЕТА ИЗОБРАЖЕНИЯ МАРКЕРА КАРЦИНОМЫ НОСОГЛОТКИ, ИСПОЛЬЗУЮЩЕГО АНТИТЕЛО, СОПРЯЖЕННОЕ С НАНОЧАСТИЦАМИ ЗОЛОТА

J.-H. Li [1*], Y. Du [2*], G.-K. Feng [2], Y.-B. Du [1], Y.-Q. Zhou [1], M.-S. Zeng [2*]

УДК 535.375.5:620.3

[1] Школа механики и электротехники, Шэньчжэньский институт информационных технологий, Шэньчжэнь, 518172, Китай; e-mail: lijianghua25@163.com
[2] Сунь Ят-Сен университетский онкологический центр, Гуанчжоу, 510060, Китай; e-mail: zengmsh@mail.sysu.edu.cn

(Поступила 22 марта 2016)

При обнаружении биомаркеров популярно использование явления поверхностного усиления комбинационного рассеяния света (SERS) на наночастицах. В настоящей работе антитело, сопряженное с наночастицами золота (AuNPs), использовано при определении LMP2A в группе клеток CNE2. Диаграммы SERS показывают наличие LMP2A в пораженной клетке, исследованной ранее методом иммунофлуоресцентного окрашивания. Это может быть обусловлено связыванием наночастиц с рецепторами поверхности клетки. При исследовании здоровых клеток CNE2 сигнал на длине волны 1044 $см^{-1}$ не обнаружен. Полученные результаты демонстрируют возможность применения AuNPs в качестве высокочувствительных зондов при обнаружении и определении места расположения маркеров карциномы носоглотки.

Ключевые слова: *карцинома носоглотки, LMP2A, маркер, наночастицы золота, CNE2.*

Introduction. Surface-enhanced Raman scattering (SERS) is popular in the imaging of biological or chemical processes occuring at the cellular level. It is reported that the SERS method yields a signal of amplitude 15 orders greater than Raman scattering and therefore allows for chemically specific imaging [1]. These narrow ‘fingerprint’ Raman spectra unique to the chemical species is called SERS-active nanoparticles (SERS nanotags) [2]. SERS nanotags are constructed by attaching strong Raman active (reporter) mole-

cules onto Au nanoparticles (AuNPs) and encapsulating them in a polyethylene glycol (PEG)/silica/bovine serum albumin shell [3, 4]. These nanotags can be easily functionalized with various receptor moieties for specific and active *in vivo* targeting of biomarkers with the following advantages: (i) multiplex detection capability due to spectral fingerprinting, (ii) low susceptibility to photo-bleaching, and (iii) low cytotoxicity due to the use of AuNPs [5]. Thus, SERS nanotags are successfully used for the early detection of cancer biomarkers [6, 7]. For example, AuNPs are used for detecting different types of cancer [8–12]. Raman reporter-labeled hollow gold nanospheres (HGNs) show much better correlations between concentration and intensity than the conventional point-based assay [13]. Histological SERS imaging may outperform conventional immunohistochemistry staining as recently described for the detection of LMP1 in nasopharyngeal tissue sections [14]. Near infrared (NIR) active SERS nanotags constructed with an Au/Ag hollow shell have also been obtained for passive *in vivo* multiplex detection when they are subcutaneously injected [15]. Recently, a fiber optic-based Raman endoscope system has been fabricated. It has the capability to detect and quantify the presence of single or multiplexed SERS nanoparticles [16].

The Epstein-Barr virus (EBV) is the first identified human tumor virus associated with various malignancies, most notably nasopharyngeal carcinoma (NPC). It is reported that LMP2A, the Epstein-Barr virus encoded latent protein, plays an essential role in oncogenic processes. Although both LMP1 and LMP2A are detectable in NPC samples, the majority of authors focus on LMP1 because of its known oncogenic properties in B cells. However, LMP2A is detected in more than 95% of NPC samples at the mRNA level, and about 50% of these specimens at the protein level, whereas LMP1 is detected only in 65/35% of NPC samples at the mRNA/protein level, respectively. In addition, the high LMP2A content in NPC samples is correlated with cellular invasion and metastasis. Thus, LMP2A can be considered as a novel target for NPC cancer [17]. Herein, LMP2A in a CNE2 cell line is analyzed on the basis of the following model. The anti-lmp2a MoAb 4A11B3A3 conjugated with AuNPs is considered as SERS substrates for LMP2A SERS imaging in a CNE2 cell line. The original CNE2 cell line without LMP2A and AuNPs is used as a control sample. The obtained SERS images are compared with the published work done by our group using immunofluorescence staining. To the best of our knowledge, this is the first report about anti-lmp2a labeled AuNPs combined with SERS imaging for detection of LMP2A.

Experimental methods. Gold nanoparticles (AuNPs) are provided by Jinan University [18]. They were prepared by reducing chloroauric acid with trisodium citrate. Briefly, 10 mL of 1% trisodium citrate was quickly added to 50 mL of the boiling chloroauric acid solution (1.0×10^{-3} M) under vigorous stirring. The color of the solution turned from pale yellow to wine red. This solution was allowed to react under heating for 15 min. When the heating mantle was removed, this solution was stirred at room temperature for another 2 h. The prepared gold colloids were stored at 4°C to maintain the stability.

Preparation of antibodies-conjugated gold nanoparticles: 1 mL of AuNPs was mixed with 200 mL of 0.2 M deoxygenated cysteamine solution for 12 h at 4°C. Cysteamine-modified AuNPs were separated by centrifugation (5000 rpm, 10 min) and washed with PBS (pH 7.4) three times to remove unimmobilized cysteamine. Amine-functional AuNPs were re-dispersed in 1 ml of PBS (pH 7.4). In order to conjugate the anti-lmp2a MoAb antibody with the AuNPs surface, 0.5 mL of the aqueous solution of 0.1 mM anti-lmp2a MoAb 4A11B3A3 was incubated with 1 mL of the cysteamine-modified AuNPs solution containing 0.25 M EDC for 12 h at 4°C. Then the antibody-conjugated AuNPs solution was separated by centrifugation (5000 rpm, 10 min) and washed three times with PBS (pH 7.4) to remove unconjugated anti-lmp2a MoAb. Finally, antibody-conjugated nanoprobes were re-dispersed in 1 mL of PBS (pH 7.4) and kept at 4°C.

LMP2A-overexpressed CNE2 cells were generated by the following methods. The poorly differentiated nasopharyngeal carcinoma cell line (CNE2) was maintained in an RPMI 1640 medium (Life Technologies, Carlsbad, CA) supplemented with 10% fetal bovine serum (FBS) in a humidified 5% CO_2 incubator at 37°C. The LMP2A monoclonal antibody was obtained from Proteintech Group Inc. ABCG2 (Cat. 3380). CNE2 cells (5×10^5) were seeded per 100-mm dish and transfected the next day with 8 μg of pCR3.1-LMP2A together with 1 μg of the EGFP-expressing vector using the FuGENE 6 reagent. EGFP positive cells were sorted out from the co-transfected cells 48 h later. To establish stably expressed LMP2A cell lines, CNE2 cells were infected with the virus expressing LMP2A in the pBabe vector, followed by selection with 0.5 μg/mL of puromycin (Sigma-Aldrich, St Louis, MO) [17].

Raman measurements. A 10-μL drop of suspended live cells in PBS was deposited on a pure aluminum flake, where the cells were allowed to settle and become immobilized after drying, ~15 μm above the aluminum surface. Raman imaging was performed using a Renishaw inVia confocal Raman system (controlled by WiRE 3.2 software) coupled with a Leica DM 2500 microscope. The spectrometer was equipped with

a 785 nm near-infrared diode laser (5 mW). A 50× objective lens (~1 μm laser spot size) was used to focus the laser beam and to collect the Raman signal. Raman spectral mapping was performed in a streamline mode at an integration time of 1 s (~0.06 s per pixel) using the point intensity at several enhance bands. The integration time for each spectrum was 1 s, and the spacing between adjacent scanning spots was 2 μm. The images of CNE2 cells were acquired after incubating with antibody-conjugated AuNPs for 2 h.

Results and discussion. The obtained assignment for the RS of the CNE2 cell line is presented in Table 1. Figure 1 shows the representative Raman spectra for CNE2 cell lines in the range 750–1750 cm^{-1} with and without antibody-conjugated AuNPs after background removal and normalization, respectively. The fluorescence background of the original data was removed using a fifth-order polynomial; the steady band at 1004 cm^{-1} assigned as phenylalanine was used for normalizing the RS curves, which enable a better comparison of the spectral shapes and relative Raman band intensities among different organs and anatomical regions [19]. It can be seen that the SERS spectra had the characteristics peak at 1044 cm^{-1} exhibiting much increased signals as compared to the CNE2 cell line; the other bands had almost the same shape with the previously obtained spectrum. Detailed band assignments are shown in Table 1 [20]. The strong band at 1044 cm^{-1} was assigned to the C-N stretching vibration in previous SERS studies [21, 22], suggesting the location of antibody-conjugated AuNPs nanotags and LMP2A infected CNE2, which might be associated with an increase in the relative amount of protein (or DNA, RNA) bases relative to the whole SERS-active constituents.

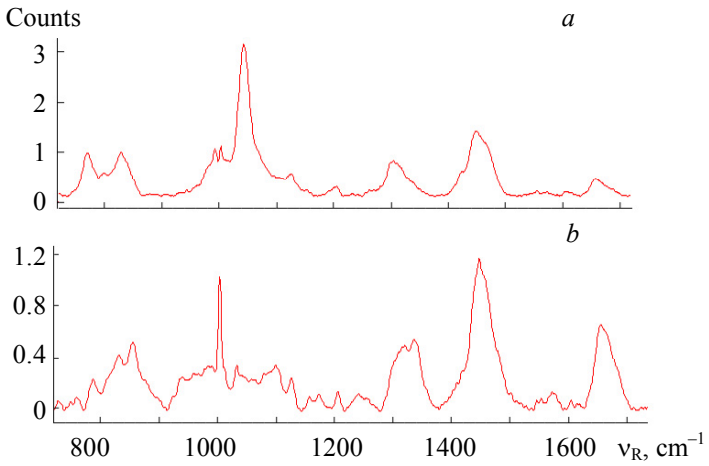

Fig. 1. SERS (a) and RS (b) antibody-conjugated AuNPs spectra of CNE2 after background removal and normalization.

TABLE 1. Band Assignment for RS of CNE2 Cell Line

ν, cm^{-1}	Assignment
784	DNA, RNA (PO_2 symmetric stretching)
830	DNA (PO_2 asymmetric stretching), tyrosine
854	ν(C–C) of proline, δ(CCH) ring breathing of collagen
940	ν(C–C) of α-helix conformation for proteins
964	Lipids, proteins (CH_3 deformation)
1004	*n*(C–C) ring breathing of phenylalanine
1033	Phenylalanine, protein C–N stretching
1044	C–N stretching vibration
1101	C–C stretching of phospholipids
1128	Protein C–N stretching
1157	DNA (ribose-phosphate)
1174	Tyrosine, phenylalanine, protein (C–H bend)
1208	Tyrosine, phenylalanine, protein (Amide III)
1320	Gyanine, protein (C–H deformation vibration)

Continue Table 1

ν, cm^{-1}	Assignment
1337	Adenine, guanine, protein (C–H deformation vibration, CH_3CH_2 twisting of nucleic acids)
1448	Lipids/pronein (CH_3 deformation, CH_2 bending)
1577	Guanine, adenine, heme C=C bending of pyrimidine ring of nucleic acids
1606	Tyrosine, phenylalanine, protein (C=C)
1619	(*n*(C=C) of porphyrins) protein
1665	Amide I ν(C=O) of proteins, α-helix conformation

The bands at 1004, 1044, 1320, and 1445 cm^{-1} are constructed and mapped in Fig. 2. The bar scales on the bottom displayed the color decoding for SERS intensity. The Raman peak intensity level at each pixel was coded by pseudo colors, black representing the lowest intensity, and red representing the highest. The Raman peak at 1004 cm^{-1} was a prominent and stable Raman signal reflecting the changes of phenylalanine. The intensities indicated the amount of phenylalanine at the spot of the cell. In the same way, the maps based on the bands at 1320 and 1445 cm^{-1} exhibited their content of protein and lipid in the cell according to Table 1. The bar scales on the right of the maps showed values different from Fig. 2. The changes of these molecular components might reflect more chemical interaction between the molecule and the microenvironment occurring in cancer cells. Interestingly, intensity mapping at 1044 cm^{-1} (Fig. 2b) showed a completely different shape from the above-mentioned maps. The Raman signal gave strong bright scattering spots on the cell surface. These bright spots were due to the light scattering property of the AuNPs in the bound nanotags. The antibody conjugated SERS nanotags bound to the biomarkers (LMP2A), which are cell membrane bound receptors, to give strong bright scattering spots on the cell surface. The map confirmed the specific interaction and binding of the bioconjugated nanotags to the biomarker on the cell surface, because LMP2A was attached to anti-lmp2a MoAb 4A11B3A3, which was conjugated to AuNPs. However, the nonconjugated nanotags did not bind to the cell surface, and thus no bright scattering spots were observed. This location was in agreement with the reported results of our immunohistochemical analysis [17], where it was said that LMP2A was mainly expressed on the CNE2 cell membrane and preferentially located at the tumor invasive front. According to the bar scale, the black color in the center still had the Raman signal, indicating that AuNPs or LMP2-AuNPs were incorporated into the cells. The representative SERS based on points *A*, *B*, *C* is shown in Fig. 3. Figure 3C shows that point *C* still had the characteristics peak at 1044 cm^{-1}, although it only had half of the intensity compared with that of point *A*. The value was consistent with the morphological brightness of Fig. 2b.

In this way, the strong and stable characteristics of SERS signals of Raman reporters in the cells demonstrate biocompatibility and stability. SERS nanotags constructed with Au nanospheres, which has the surface plasmon resonance in the NIR range coupled with the plasmonic heating associated photothermal property,

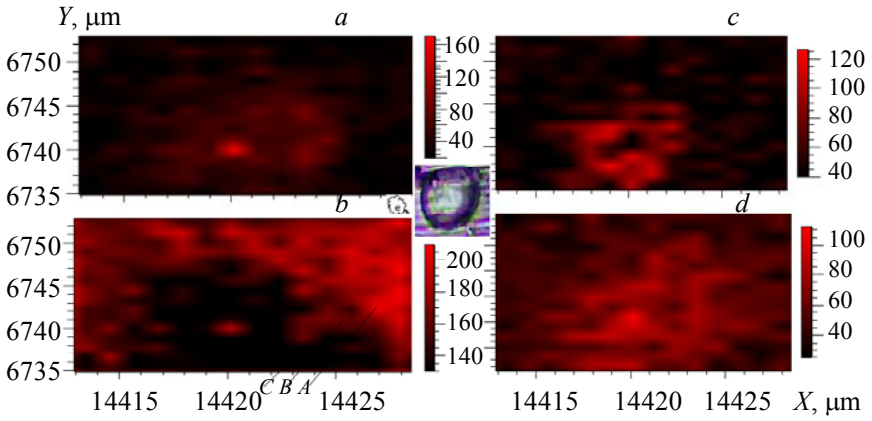

Fig. 2. SERS mapping results with SERS nanotags demonstrating the expression and relative distribution of the biomarkers (LMP2A) on the cell surface bound to the antibody-conjugated SERS nanotags (anti-lmp2a MoAb 4A11B3A3), map at 1004 (a), 1044 (b), 1320 (c), and 1450 cm^{-1} (d); the bright field of CNE2 with antibody-conjugated AuNPs (e).

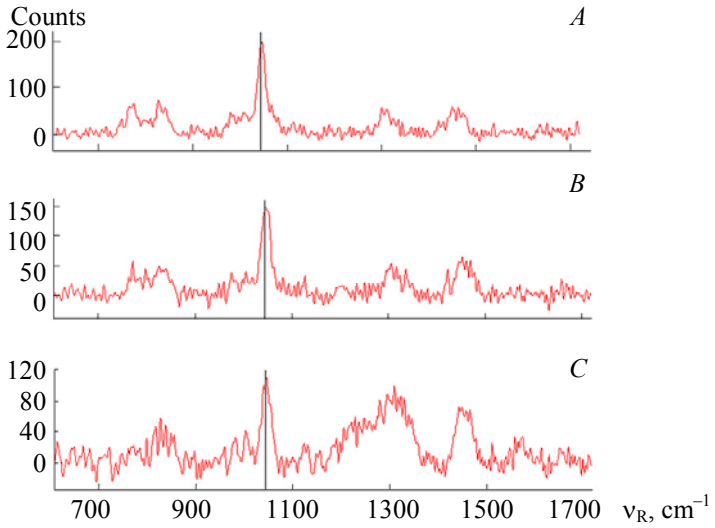

Fig. 3. SERS spectra from LMP2A-CNE2 cell line showing the peaks at 1044 cm^{-1} from nonbioconjugated SERS nanotags corresponding to points *A*, *B*, and *C* in Fig. 2b respectively. Signal intensity gave an enhancement of two orders of magnitude from the cell membrane to cell.

can be employed in developing these particles as sensitive theranostic probes. Such probes will find application in efficient cancer detection and therapy, especially when SERS tags are administered to bind to multiple biomarkers on cancer cells.

The location of cancer biomarkers using biocompatible SERS nanotags has recently emerged as the most promising tool for biosensing and imaging by the characteristics spectra. SERS nanotags with antibodies specifically interacted and actively bound to their receptors and thus contributed to the prolonged signal at the tumor site, whereas SERS nanotags without antibodies dissipated fast from the tumor site. This way, these tags can be used to quantify the levels of biomarkers and thus monitor the cancer progression or the therapy effectiveness.

LMP2A plays an important role in oncogenic processes. It was reported that LMP2A was observed in 57.6% of NPC tumor samples. It was mainly localized at the tumor invasive front. Moreover, the larger the LMP2A amount in NPC samples, the worse the prospect of survival. In addition, LMP2A dramatically affects the properties of epithelial cells: their ability to accelerate anchorage-independent growth, promote tumor growth in nude mice, and activate cell motility. On the other hand, LMP2A strongly upregulates the cancer stem cell-like population in NPC, which can explain the onset of metastases and the high rate of recurrence for these tumors. This raises the possibility that this viral protein plays a key role not only in EBV latency and persistence but also in the progression of NPC. Thus, the detection of LMP2A in tumor tissues is important in predicting the NPC progression, and LMP2A can be considered as a novel therapeutic target for this cancer [23, 24].

The results of the investigation of NPC patients' biopsies revealed that for 19 out of 33 (57.6%) paraffin-embedded samples it showed moderate to strong staining of LMP2A in most of the tumor cells and scattered infiltrated lymphocytes in some of them. No positive staining was detected in adjacent noncancerous epithelial cells [17]. LMP2A is detected in NPC samples at various levels. Its localization at the invasive front indicates a potential role in promoting tumor invasion. From nude mice inoculated with CNE2-LMP2A cells, we established a level of LMP2A that was comparable to that found for the NPC biopsies. Hence, physiological levels of LMP2A can exist. Thus, further studies of LMP2A function are necessary. Thus, LMP2A-infected CNE2 cells were applied to simulate the NPC tissue; and clone MoAb 4A11B3A3, which was anti-lmp2a, was attached to AuNPs for detecting the biomarker (LMP2A). Thus, the level of LMP2 markers (protein) proteins is the main reason to change the shape of the spectra. SERS with antibody-conjugated AuNPs is emerging as a powerful new tool for targeting and imaging specific cancer markers in living cells.

To our knowledge, this is the first report to locate LMP2A, can be used as a biomarker of NPC from the LMP2A-infected CNE2 cell line by conjugating the anti-lmp2a MoAb 4A11B3A3 to AuNPs. In our measurement, a characteristics peak at 1044 cm^{-1} was detected, which did not exist in the RS of CNE2, suggesting

the peak is caused by AuNPs. Because LMP2A-infected CNE2 can conjugate to anti-lmp2a MoAb 4A11B3A3, which is connected with AuNPs, LMP2A can be obtained from the intensity of the peak at 1044 cm^{-1}. What's more, the Raman imaging constructed by the band at 1044 cm^{-1} demonstrated that the intensity in each cell was enhanced, but cell membrane was brighter than the center, suggesting that LMP2A located mostly at the cell membrane. The result agreed with our previous report using immunofluorescence staining with four different LMP2A MoAb clones [17]. Our findings are in agreement with the previous observation of a direct SERS and can provide detailed information for cell biologists.

Conclusion. We considered the LMP2A biomarker a novel target for NPC diagnostics using SERS nanotags. The characteristics peak at 1044 cm^{-1} was observed from the SERS, which did not exist in the RS of the CNE2 cell line. The SERS map at 1044 cm^{-1} demonstrated the brighter scattering spot around the cell, suggesting the membrane localization of LMP2A in the LMP2A-infected NPC cells, because the anti-lmp2a MoAb 4A11B3A3 attached to AuNPs. The light distributions were consistent with the results obtained by immunofluorescence staining. The detection of LMP2A by SERS specific nanotags can be useful in predicting NPC progression.

Acknowledgment. This work was funded by the National Natural Science Foundation of China (31200629), Science and Technology Planning Project of Guangdong Province (2015A050502006), and the Shenzhen Science and Technology Innovation Committee (JCYJ20150417094158018, GJHZ20150316112419786, and JCYJ20150417094158016).

REFERENCES

1. L. S. Lawson, J. W. Chan, T. Huser, *Nanoscale*, **6**, 7971–7980 (2014).
2. U. S. Dinish, G. Balasundaram, Y. Chang, O. Malini, *Sci. Rep.*, **4**, 4075 (2014).
3. K. K. Maiti, U. S. Dinish, C. Y. Fu, J. J. Lee, K. S. Soh, S. W. Yun, R. Bhuvaneswari, M. Olivo, Y. T. Chang, *Biosens. Bioelectron.*, **26**, 398–403 (2010).
4. A. Samanta, K. K. Maiti, K. S. Soh, X. Liao, M. Vendrell, U. S. Dinish, S. W. Yun, R. Bhuvaneswari, H. Kim, S. Rautela, J. Chung, M. Olivo, Y. T. Chang, *Angew. Chem. Int. Ed.*, **50**, 6089–6092 (2011).
5. W. Xie, L. Su, A.Shen, A.Materny, J. Hu, *J. Raman Spectrosc.*, **42**, 1248–1254 (2011).
6. U. S. Dinish, G. Balasundaram, Y. T. Chang, M. Olivo, *J. Biophoton*., 7, No. 11-12, 956–965 (2014).
7. M. Vendrell, K. K. Maiti, K. Dhaliwal, Y. T. Chang, *Trends Biotechnol.*, **31**, 249–257 (2013).
8. K. K. Maiti, A. Samanta, M. Vendrell, K. S. Soh, M. Olivo, Y. T. Chang, *Chem. Commun.*, **47**, 3514–3516 (2011).
9. M. K. Gregas, J. P. Scaffidi, B. Lauly, T. Vo-Dinh, *Appl. Spectrosc.*, **64**, No. 8, 858–866 (2010).
10. J. Yang, Z. Wang, X. Tan, J. Li, C. Song, R. Zhang, Y.Cui, *Nanotechnology*, **21**, 345101 (2010**)**.
11. K. Ock, W. I. Jeon, E. O. Ganbold, M. Kim, J. Park, J. H. Seo, K. Cho, S. W. Joo, S. Y. Lee, *Anal. Chem.*, **84**, 2172–2178 (2012).
12. B. Yan, Y. Hong, T. Chen, B. M. Reinhard, *Nanoscale*, **4**, 3917–3925 (2012).
13. M. Lee, S. Lee, J. H. Lee, H. W. Lim, G. H. Seong, E. K. Lee, S. I. Chang, C. H. Oh, J. Choo, *Biosens. Bioelectron.*, **26**, 2135–2141 (2011).
14. Y. Chen, X. Zheng, G. Chen, C. He, W. Zhu, S. Feng, G. Xi, R. Chen, F. Lan, H. Zeng, *Int. J. Nanomed.*, **7**, 73–82 (2012).
15. H. Kang, S. Y. Jeong, Y. G. Park, J. Yim, B. H. Jun, S. Kyeong, J. K. Yang, G. S. Kim, S. G. Hong, L. P. Lee, J. H. Kim, H. Y. Lee, D. H. Jeong, Y. S. Lee, *Adv. Funct. Mater.*, **23**, 3719–3727 (2013).
16. C. L. Zavaleta, E. Garai, J. T. Liu, S. Sensarn, M. J. Mandella, D. Van de Sompel, S. Friedland, J. Van Dam, C. H. Contag, S. S. Gambhir. *Proc. Natl. Acad. Sci. USA*, **110**, E2288–E2297 (2013).
17. K. Q. Li, L. J. Hu, J. Y. Cao, G. K. Feng, *PLoS Pathogens*, **6**, No. 6, e1000940 (2010).
18. H. H. Cai, P. H. Yang, J. Feng, J. Cai, *Sens. Actuat. B: Chem.*, **135**, 603–609 (2009).
19. X. L. Yan, R. X. Dong, L. Zhang, X. J. Zhang, Z. W. Zhang, *World J. Gastroenterol.*, **11**, No. 21, 3290–3292 (2005).
20. J. H. Li, W. T. Li, G. H. Zhang, *Laser Phys.*, **24**, 12560 (2014).
21. P. D. Bao, T. Q. Huang, X. M. Liu, T. Q. Wu, *J. Raman Spectrosc.*, **32**, No. 32, 227–230 (2001).
22. S. Stewart, P. M. Fredericks, *Spectrochim. Acta, A*, **55**, 1615 (1999).
23. N. Heussinger, M. Buttner, G. Ott, E. Brachtel, B. Z. Pilch, E. Kremmer, G. Niedobitek. *J. Pathol.*, **203**, 696–699 (2004).
24. D. M. Pegtel, A. Subramanian, T. S. Sheen, C. H. Tsai, T. R. Golub, D. A. Thorley-Lawson, *J. Virol.*, **79**, 15430–15442 (2005).